Crystal architectures of a layered silicate on monodisperse spherical silica particles cause the topochemical expansion of the core-shell particles

Tomohiko Okada, [a]* Asuka Suzuki, [a] Shiho Yoshido [a] and Hikari M. Minamisawa [b]

[a] *Department of Chemistry and Material Engineering, Faculty of Engineering, Shinshu University, Wakasato 4-17-1, Nagano 380-8553, Japan*

[b] *Technology Division, Faculty of Engineering, Shinshu University, Wakasato 4-17-1, Nagano 380-8553, Japan*

* Corresponding author: Tomohiko Okada

Phone : +81-26-269-5414, Fax : +81-26-269-5424,

e-mail: tomohiko@shinshu-u.ac.jp

Abstract

Anisotropic structural changes in an expandable layered silicate (directed towards the *c*–axis) occurring on isotropic and monodisperse microspheres were detected by measurable increases in the grain size. The hierarchical changes were observed through pursing the sophisticated growth of expandable layered silicate crystals on monodisperse spherical

silica particles with diameters of 1.0 μm; the core–shell hybrids with a quite uniform grain size were successfully produced using a rotating Teflon-lined autoclave by reacting spherical silica particles in a colloidal suspension with lithium and magnesium ions under alkaline conditions at 373 K. The size distribution of the core-shell particles tended to be uniform when the amount of lithium ions in the initial mixture decreased. The intercalation of dioctadecyldimethylammonium ions into the small crystals through cation-exchange reactions expanded the interlayer space, topochemically increasing the grain size without any change occurring in the shapes of the core–shell particles.

Keywords: Colloidal silica, Layered silicate, Cation exchange, Layer charge density, Hierarchical hybridization

1. Introduction

It is an attractive proposition to use the expandable two-dimensional nanospaces in layered materials to organise guest organic species to add to the possibilities that are already available, which are to use ordered and constrained nano-environments and well-established nanoporous materials (e.g. zeolites and mesoporous solids).[1–4] Inorganic–organic periodic materials such as metal–organic frameworks, porous coordination polymers[5,6] and crystal-like periodic organosilicas,[7,8] have been of increasing interest because the organic moieties are spatially arranged in regular patterns in these materials. Nanosheet components have recently been used as scaffolds to create nanospaces to accommodate guest species.[9,10] However, nano-architectures involving the intercalation

of organic moieties into two-dimensional expandable interlayer spaces in inorganic layered solids have long been studied. Nanospaces in interlayer space have been controlled by controlling the spatial distributions of the organic moieties by varying the numbers, positions and sizes (molecular geometries) of the organic moieties.[11–17] This nanostructural versatility has encouraged us to seek further applications for these systems in selective adsorption, separation, catalysis and photochemical reactions.[16]

The smectite group of layered clay minerals has been more extensively studied than have other layered inorganic solids.[18,19] Smectites are composed of ultrathin (*ca*. 1.0 nm) crystalline silicate layers separated by hydrated interlayers.[19,20] A silicate layer is composed of two silicon tetrahedral sheets and one aluminium (or magnesium) octahedral sheet. A negative charge in a silicate layer, generated through isomorphous substitution (e.g. the substitution of Si^{4+} with Al^{3+} in a tetrahedral sheet or of Mg^{2+} with Li^{+} in an octahedral sheet), will be compensated for by the presence of an interlayer alkali metal cation. Cation-exchange reactions between the interlayer cations and organoammonium ions are well known, and they are used in such applications as modifying surfaces, producing hydrophobic and microporous inorganic–organic hybrids for the uptake of specific molecules,[21,22] producing controlled release materials, achieving selective catalysis and achieving efficient photo-induced processes.[16,23] The cation exchange capacity (CEC), which directly correlates with the negative-layer charge density, is an important determiner of the distance between adjacent interlayer cations (the spatial density). Achieving an appropriate distance can allow the material to act as a molecular sieve for nonionic organic compounds[24–29] or to improve the photofunctions of photoactive molecules.[30–34] It

has therefore been recognised that one of the advantages smectites offer (in addition to the many other important properties of smectites and their intercalation compounds) is that the CEC can be varied in order to control the spatial distribution of organic moieties.[35] Hectorite[36] and saponite[37] are layered clay minerals in the smectite family that have variable CECs. Hectorite and saponite have been synthesised for use precisely controlling cationic dye distributions[37] and adsorbing organic molecules.[38]

The ability to control the morphology (i.e., grain size and shape) of a smectite is vital to achieving the optimum performance of a molecularly recognizable smectite-based hybrid. Quite fine crystals of synthetic smectites are generally obtained.[39,40] The shapes required have been produced through the bottom-up self-assembly of silicate layers by freeze-drying hydrogels,[41–43] moulding non-cordierite honeycomb monoliths[44] and using optically transparent films[45–48] fabricated using various techniques (including depositing a smectite suspension on a substrate, using the Langmuir–Blodgett technique to exfoliate platelets[49–51] and using a layer-by-layer deposition technique[52–54]). The deposition of smectite silicate layers on different particles using an alternating adsorption technique[55] has recently allowed another class of multifunctional materials with hierarchical hybridizations to be produced. We have described the *in situ* crystallization of a smectite-like layered silicate on spherical silica particles. In that process the silica particles were found to be consumed through hydrothermal reactions without losing the silica morphology, and the silica that was consumed was found to be used as the source of the smectite.[56] Core–shell hybridization is not like the *papier mâché* method (but the so-called sacrificial template or self-template method), and it is possible to avoid flakes falling

off the silica particles even in aqueous media. The monodisperse core–shell particles produced using the sacrificial template method could be used as host materials and/or building units in future separation, sensor, optics and electronic applications because the periodic arrangement of smectite (or a related layered solid) particles with defined shapes is key to achieving more sophisticated functional materials.[57,58]

Here, we describe the sophisticated crystal growth of a hectorite-like layered silicate (abbreviated to Hect) with the ideal formula $Li_x(Mg_{6-x}Li_xSi_8O_{20}(OH)_4)\cdot nH_2O$ on monodisperse amorphous spherical silica particles (abbreviated to Silica@Hect) using a sacrificial template method. Changing the LiF/$MgCl_2$ molar ratio in the starting mixture allowed the size of the Hect on the silica to be the negative-layer charge density of the Hect on the silica to be varied, from 0.5 to 0.9 mEq/g of Hect. The topochemical expansion of the Silica@Hect core–shell particles occurred when cationic surfactants were intercalated into the Hect via ion-exchange reactions.

2. Experimental section

2.1. Materials.

Lithium fluoride, magnesium dichloride hexahydrate, urea, dioctadecyldimethylammonium (abbreviated to $2C_{18}$) bromide, and methylene blue (abbreviated to MB) were purchased from Wako Pure Chemical Ind., Ltd. Monodispersed spherical silica powder with the grain

size of 1.0 μm (KE–S100, Nippon Shokubai Co., Ltd.) was used as the source of hectorite-like silicate. All these chemicals were used without further purification.

2.2. Fabrication of Silica@Hect core–shell particles.

A typical procedure was reported that described in the previous paper.[56] Here we modified the hydrothermal reaction conditions including chemical compositions and the heat treatment. A typical example of the LiF:$MgCl_2$:SiO_2:urea molar ratio in the starting mixture was 0.21:0.8:8.0:8.0, where the amounts of the Li and Mg sources added relative to the amount of SiO_2 were decreased by 15% from the Li:Mg:Si ratio of 1.4:5.6:8.0 [36]. Urea (2.16 g), $MgCl_2 \cdot 6H_2O$ (0.73 g) and LiF (0.024 g) were dissolved in water (80 mL). The resulting solution was mixed with an aqueous suspension of spherical silica particles (2.16 g in 20 mL of water) using a mechanical homogenizer (at 4600 revolutions per minute) for 30 min at room temperature. The slurry was transferred to a Teflon-lined autoclave and heated to 373 K for 48 h. The autoclave was rotated at 15 revolutions per minute using a hydrothermal synthesis reactor unit (Hiro Company) during the heat treatment. The slurry was then cooled in an ice bath and centrifuged (at 1400 g for 20 min), then the precipitate was collected and dried at 323 K. The LiF:$MgCl_2$:SiO_2 molar ratio in the starting mixture was changed as summarised in Table 1 to vary the CEC of the product.

2.3. Adsorption isotherms of MB on Silica@Hect from aqueous solution.

Silica@Hect core–shell particles (0.05 g) were reacted with 20 mL of aqueous MB solution (0.13–0.75 mM) in a glass vessel with magnetic stirring for 1 day at 25 °C. To estimate the adsorption of MB to the vessel, blank samples containing 20 mL of aqueous MB solution

with no adsorbents were also prepared. After centrifugation (1400 *g*, 20 min), the concentration of MB remaining in the supernatant was determined by Vis. spectroscopy (λ = 665 nm).

2.4. Cation-exchange reactions of Silica@Hect with a cationic surfactant.

$2C_{18}$ bromide (15 mg) in a mixture of water and ethanol (10 mL, 50/50 *v*/*v*) was allowed to react with Silica@Hect (0.1 g) by magnetic stirring at room temperature for 1 day. The product was collected by centrifugation (1400 *g* for 20 min); this was followed by repeated washing with the mixture of water and ethanol. Finally, the washed solid was dried at 323 K.

2.5. Equipments.

X-Ray powder diffraction (XRD) patterns were obtained by a Rigaku RINT 2200V/PC diffractometer (monochromatic Cu Kα radiation), operated at 20 mA, 40 kV. Thermogravimetric-differential thermal analysis (TG-DTA) curves were recorded on a Rigaku TG8120 instrument at a heating rate of 10 K/min and using α-alumina as the standard material. Nitrogen adsorption-desorption isotherms were measured at 77 K on Belsorp–mini (BEL Japan, Inc.). Before the adsorption experiment, the samples were heat-treated at 393 K under a reduced pressure. Scanning electron micrographic (SEM) images were captured on Hitachi SU-8000 field-emission scanning electron microscope (operated at 1 kV) after dealing with osmium plasma coating to the samples. Transmission electron micrographic (TEM) observations were conducted by using Hitachi HighTech HD–2300A scanning transmission electron and JEOL JEM–2010 transmission electron microscopes,

whose accelerated voltage is 200 kV. UV–Vis spectra were recorded on a Shimadzu UV–2450PC spectrophotometer.

3. Results and Discussion

Fig. 1 shows SEM images of the Silica1.0@HectX (X = 1, 2, 3 and 4) and raw spherical silica particles. The Silica1.0@HectX particles were basically spheres. The surfaces of the silica particles were smooth but the surfaces of the Silica1.0@HectX particles were rough, with fine plate-like particles developing perpendicular to the silica substrate surfaces. We found that the surfaces of the spherical silica grains were thoroughly and homogeneously covered with the fine plat-like particles irrespective of the Li/Mg ratio in the starting mixture.

The cross-sectional TEM images of the Silica1.0@HectX samples (on the right in Fig. 1) show that there were stacked and/or agglomerated layers around the silica core, whereas the original silica was smooth. Roughness was shown at the interface between the crystal layers and the residual silica core, indicating that the silica had been partially eroded during the hydrothermal reaction. The powder XRD patterns of the samples (Fig. 2) showed reflection peaks that were ascribed to hectorite at 8° (2θ Cu Kα) for (*001*), 35° (2θ) for (*130*) and 61° (2θ) for (*060*). The stacked layers observed were therefore regarded as hectorite-like layered silicate crystals. The crystal domain was very thin in the Silica1.0@Hect1 and Silica1.0@Hect2 samples. A low-density amorphous substance (the bright area in the TEM image) about 20 nm thick was found between the silica core and the

layer aggregate. We deduced from the TEM observations that the hectorite-like silicate grew from the low-density substance. As is shown in the Z-contrast image (see the Supplementary data Fig. S1), this unique structure was observed in every particle in each sample.

We assumed that the layered silicate formed through heterogeneous nucleation on the silica surface in water.[56] Hydroxyl ions evolved through the hydrolysis of urea would yield both a water-soluble Mg–Li double hydroxide (or partial $Mg(OH)_2$), produced from the Mg^{2+} and Li^{+} ions in the aqueous medium, and silicate anions supplied through the partial dissolution of the spherical silica particles. These substances would be the sources of the nuclei. The layered silicate crystals would have grown on the silica surfaces because cooling caused the solution to become supersaturated. The crystal domain tended to increase in size when the amount of LiF added was increased (Silica1.0@Hect3 and Silica1.0@Hect4), as shown in the SEM and TEM images (Fig. 1). The stacked layers would readily have bent and partly grown towards the outside of the silica surfaces because of the flexibility of the silicate layer. The crystal growth led to protrusions forming on the surfaces, as shown in the SEM images.

The grain size distributions determined from the SEM images are also shown in Fig. 1. The mean sizes of the Silica1.0@Hect1 and Silica1.0@Hect2 grains were 1.16±0.02 and 1.13±0.03 μm, respectively, and these were slightly larger than the silica particles (1.00±0.02 μm). We found that the size distribution of the resulting sample particles was quite uniform as a result of few hectorite crystallites derived from homogeneous nucleation. Performing a hydrothermal reaction without rotating the reactor caused the distribution to

be broad because large hectorite protrusions were formed, as shown in the SEM image (see Supplementary data Fig. S2). No individual hectorite crystallites produced by homogeneous nucleation were observed when the reactions to give Silica1.0@Hect3 and Silica1.0@Hect4 were performed while the reactor was rotated. However, it was difficult to determine the average size of the whole grains because of the large protrusions on the surfaces. Nitrogen adsorption-desorption isotherms for the Silica1.0@HectX samples are shown in Fig. 3. Each adsorption isotherm was of type II with a hysteresis loop, suggesting the formation of the mesopores at the grain boundary of the Hect crystallites. The specific surface areas obtained from Branauer–Emmett–Teller[59] plots were relatively small for Silica1.0@Hect3 (13 m^2/g) and Silica1.0@Hect4 (9 m^2/g) compared to the specific surface areas of Silica1.0@Hect1 and Silica1.0@Hect2, which were 33 and 20 m^2/g, respectively.

The adsorption of a cationic dye, methylene blue (MB), from an aqueous solution by the Silica1.0@HectX (X = 1, 2, 3 and 4) samples was examined. The adsorption of MB by smectites, including hectorite, has previously been used for such purposes as determining the CEC[60] and identifying the spectroscopic properties of the adsorbed MB.[61,62] Fig. 4 shows the isotherms for the adsorption of MB to the Silica1.0@HectX samples from aqueous solutions. The isotherms were type L, according to the Giles[63] classification. The adsorption isotherms fitted the Langmuir equation[64] shown in Eq. 1,

$$C_e/Q = (1/K_L Q_m) + (1/Q_m)C_e, \quad (1)$$

where Q_m and K_L are constants related to the maximum amount adsorbed and the binding energy, respectively. Q and C_e are the amounts of MB adsorbed and the equilibrium concentration, respectively. The Langmuir parameters derived from the adsorption isotherms are presented in Table 2. The Q_m value increased as the Li/Mg ratio in the starting mixture increased. Electrostatic interactions between the Hect and MB were, in addition to dye–dye interactions (aggregation), a dominant role in the adsorption of MB.

We examined the quantitative ion-exchange reactions between the interlayer-exchangeable cations in Silica1.0@HectX (X = 1, 2, 3 and 4) and a cationic surfactant, $2C_{18}$. The TG curves of the $2C_{18}$-intercalated products are shown in Fig. 5. An exothermic peak was observed in the temperature range 473–673 K in each DTA curve (see Supplementary data Fig. S3), and this peak was accompanied by mass loss in the corresponding TG curve (as shown in Table 2). The amount of $2C_{18}$ that was adsorbed was determined, from the mass loss measured, to be 0.11–0.21 mmol/g (Table 2). The amount of $2C_{18}$ adsorbed increased as the amount of LiF added to the starting mixture was increased.

The quantitative exchange of alkylammonium ions can be used to determine the negative-layer charge density in smectites.[23,36,65–67] The amount of intercalated alkylammonium ions can be deduced from changes in the basal spacings caused by the intercalating alkylammonium ions, the arrangement as a function of the layer charge density and the alkyl chain length. The arrangement will change from the parallel type (monomolecular, bimolecular and *pseudo*-trimolecular layers, with the alkyl chains parallel to the silicate layers) to the paraffin type in the interlayer space [67, 68] as the layer charge density of a smectite is increased, as shown schematically in Fig. 6. Fig. 7 shows the

changes found in the XRD patterns when $2C_{18}$ exchange occurred. The basal spacing increased from 1.3 nm to 1.9, 2.3, 2.2 and 2.5 nm when exchange occurred in Silica1.0@Hect1, Silica1.0@Hect2, Silica1.0@Hect3 and Silica1.0@Hect4, respectively. The interlayer space (Δd) was determined by subtracting the thickness of the silicate layer (1.0 nm) from the observed basal spacing. A methylene group is 0.4 nm thick, so the Δd of 0.9 nm indicated that the $2C_{18}$ molecules were arranged in bimolecular layers (on the left in Fig. 6). *Pseudo*-trimolecular layer arrangements (shown in the middle of Fig. 6) were plausible in the Silica1.0@Hect2 and Silica1.0@Hect3 samples because the Δd values were 1.2–1.3 nm. We concluded that the paraffin-type arrangement [67, 68] occurred in Silica1.0@Hect4 because Δd was 1.5 nm. These observations clearly reveal that the fine Hect crystals on the silica spheres had layer charge densities that varied depending on the Li/Mg molar ratio in the starting mixture. The estimated negative-layer charge density of Hect on the silica was 0.5–0.9 mmol/g, according to a report on the $2C_{18}$ intercalation.[36]

Fig. 8 shows how the size distribution of the Silica1.0@Hect1 particles changed when the particles underwent cation exchange with $2C_{18}$. The intercalation of $2C_{18}$ into Silica1.0@Hect1 increased the mean size from 1.16±0.02 to 1.20±0.04 μm, measured from the SEM images acquired *in vacuo*. The Δd was 0.9 nm after $2C_{18}$ had become intercalated, and the grain size increased by 0.04 μm; so an average of *ca*. 40 silicate sheets were estimated to be present on each silica core. This estimate reflected the observed thickness of the hectorite shell (several tens of nanometres) determined from the cross-sectional TEM image (the magnified image is shown in Supplementary data Fig. S4).

The behaviours of the materials presented here are the first examples, to the best of our knowledge, of anisotropic structural changes (directed towards the *c*–axis) occurring on isotropic and monodisperse microspheres that can be detected by measurable increases in the grain size. Some examples have been found of morphological changes in organic–inorganic hybrid films in response to nano-structural changes that can be detected using XRD and that are accompanied by the expansion and/or contraction of the interlayer space.[15,69,70,71] These responses are worth investigating because they could be used in such applications as sensors and optics driven by interlayer structural changes.

4. Conclusions

The *in situ* crystallization of a fine Hect was performed on monodispersed spherical silica particles with diameters of 1.0 μm when the particles reacted hydrothermally with LiF and $MgCl_2$ in the presence of urea at 373 K in a rotating Teflon-lined autoclave. The surfaces of the spherical silica grains were thoroughly and homogeneously covered with the fine plat-like Hect crystals. The negative-layer charge density of Hect, estimated from the results of adsorption experiments using MB and $2C_{18}$, was 0.5–0.9 mmol/g of Hect and depended on the amounts of LiF and $MgCl_2$ that were present in the starting mixture. The crystal domain tended to be thin when the layer charge density of the Hect was small. Thus, the core–shell samples had quite uniform size distributions. The intercalation of $2C_{18}$ into the Hect with small layer charge density through cation-exchange reactions increased the interlayer space; this was accompanied by the grain size increasing topochemically without any change

occurring in the shapes of the Silica@Hect core–shell particles. The heterogeneous nucleation of fine Hect crystallites onto monodisperse spherical silica particles using LiF and $MgCl_2$ was, therefore, shown to be important in terms of the topochemical morphological changes that were induced by nanostructural changes that were detectable by XRD.

Appendix A. Supplementary data

Supplementary data related to this article can be found at http://dx.doi.org/…

Acknowledgment

This work was financially supported by JSPS KAKENHI (Grant-in-Aid for Scientific Research, Grant 26810121), the Cosmetology Research Foundation, and by JGC-S Scholarship Foundation.

References

[1] Solid-State Supramolecular Chemistry: Two- and Three-Dimensional Inorganic Networks, G. Alberti, T. Bein, Eds., Pergamon, Oxford, 1996.

[2] Stein, Adv. Mater.15 (2003) 763.

[3] E. Ruiz-Hitzky, P. Aranda, N. Darder, M. Ogawa, Chem. Soc. Rev. 40 (2011) 801.

[4] K. Ariga, A. Vinu, Y. Yamauchi, Q. Li, J. P. Hill, Bull. Chem. Soc. Jpn. 85 (2012) 1.

[5] M. Yaghi, H. Li, C. Davis, D. Richardson, T. L. Groy, Acc. Chem. Res. 31 (1998) 474.

[6] S. Kitagawa, R. Kitaura, S. Noro, Angew. Chem. Int. Ed., 43 (2004) 2334.

[7] S. Fujita, S. Inagaki, Chem. Mater. 20 (2008) 891.

[8] K. Kuroda, A. Shimojima, K. Kawahara, R. Wakabayashi, Y. Tamura, Y. Asakura, M. Kitahara, Chem. Mater. 26 (2014) 211.

[9] J. Park, D. Yuan, K. T. Pham, J. R. Li, A. Yakovenko, H. C.; Zhou, J. Am. Chem. Soc. 134, (2012) 99.

[10] N. Yanai, T. Uemura, M. Inoue, R. Matsuda, T. Fukushima, M. Tsujimoto, S. Isoda, S. Kitagawa, J. Am. Chem. Soc. 134 (2012) 4501.

[11] R. M. Barrer, Zeolites and Clay Minerals as Sorbents and Molecular Sieves, Academic Press, London, 1978.

[12] M. Ogawa, K. Kuroda, Chem. Rev. 95 (1995) 399.

[13] Handbook of Layered Materials; S. M. Auerbach, K. A. Carrado, P. K. Dutta, Eds., Marcel Dekker, 2004.

[14] Y. Ide, M. Sadakane, T. Sano, M. Ogawa, J. Nanosci. Nanotechnol. 14 (2014) 2135.

[15] T. Okada, M. Ogawa, Clay Sci. 15 (2011) 103.

[16] T. Okada, Y. Ide, M. Ogawa, Chem.–Asian J. 7 (2012) 1980.

[17] S. Takagi, T. Shimada, Y. Ishida, T. Fujimura, D. Masui, H. Tachibana, M. Eguchi, H. Inoue, Langmuir 29 (2013) 2108.

[18] B. K. G. Theng, The Chemistry of Clay-Organic Reactions, Adam Hilger; London, 1974.

[19] Handbook of Clay Science (Developments in Clay Science, Vol. 1), F. Bergaya, B. K. G. Theng, G. Lagaly, Eds., Elsevier, Amsterdam, 2006.

[20] H. van Olphen, An Introduction to Clay Colloid Chemistry 2nd ed., Wiley–Interscience, New York, 1977.

[21] R. M. Barrer, Clays Clay Miner. 37 (1989) 385.

[22] S. Xu, G. Sheng, S. A. Boyd, Adv. Agron. 59 (1997) 25.

[23] T. Okada, Y. Seki, M. Ogawa, J. Nanosci. Nanotech. 14 (2014) 2135.

[24] W. F. Jaynes, S. A. Boyd, Clays Clay Miner. 39 (1991) 428.

[25] M. A. M. Lawrence, R. K. Kukkadapu, S. A. Boyd, Appl. Clay Sci. 13 (1998) 13.

[26] T. Okada, M. Ogawa, Chem. Commun. (2003) 1378.

[27] T. Okada, M. Ogawa, Bull. Chem. Soc. Jpn. 77 (2004) 1165.

[28] T. Okada, T. Morita, M. Ogawa, Appl. Clay Sci. 29 (2005) 45.

[29] T. Okada, J. Oguchi, K. Yamamoto, T. Shiono, M. Fujita, T. Iiyama, Langmuir 31 (2015) 180.

[30] M. Ogawa, T. Aono, K. Kuroda and C. Kato, Langmuir, 1993, 9, 1529–1533.

[31] M. Ogawa, R. Kawai, K. Kuroda, J. Phys. Chem. 100 (1996) 16218.

[32] S. Takagi, T. Shimada, M. Eguchi, T. Yui, H. Yoshida, D. A. Tryk, H. Inoue, Langmuir 18 (2002) 2265.

[33] T. Okada, Y. Watanabe, M. Ogawa, J. Mater. Chem. 15 (2005) 987.

[34] J. Bujdak, V. M. Martinez, F. L. Arbeloa, N. Iyi, Langmuir 23 (2007) 1851.

[35] Layer Charge Characteristics of 2:1 Silicate Clay Minerals, A. R. Mermut, Ed., CMS workshop lectures vol. 6, Clay Minerals Society, 1994.

[36] M. Ogawa, T. Matsutomo, T. Okada, J. Ceram. Soc. Jpn. 116, (2008) 1309.

[37] T. Egawa, H. Watanabe, T. Fujimura, Y. Ishida, M. Yamato, D. Masui, T. Shimada, H. Tachibana, H. Yoshida, H. Inoue, S. Takagi, Langmuir 27 (2011) 10722.

[38] T. Okada, T. Matsutomo, M. Ogawa, J. Phys. Chem. C 114 (2010) 539.

[39] J. T. Kloprogge, S. Komarneni, J. E. Amonette, Clays Clay Miner. 47 (1999) 529.

[40] K. A. Carrado, Appl. Clay Sci., 2000 17 (2000) 1.

[41] F. Call, Nature 172 (1953) 126.

[42] T. J. Pinnavaia, M.-S. Tzou, S. D. Landau, R. H. Raythatha, J. Mol. Catal. 27 (1984) 195.

[43] T. Okada, T. Kato, T. Yamaguchi, T. Sakai, S. Mishima, Ind. Eng. Chem. Res. 52 (2013) 12018.

[44] J. M. Gatica, H. Vidal, J. Hazardous Mater. 181 (2010) 9.

[45] M. Ogawa, M. Takahashi, C. Kato, K. Kuroda, J. Mater. Chem. 4 (1994) 519.

[46] R. Sasai, N. Iyi, T. Fujita, L. F. Arbeloa, M. V. Martinez, K. Takagi, H. Itoh, Langmuir 20 (2004) 4715.

[47] S. Takagi, T. Shimada, D. Masui, H. Tachibana, Y. Ishida, D. A. Tryk, H. Inoue, Langmuir 26 (2010) 4639.

[48] J. Kawamata, Y. Suzuki, Y. Tenma, Philos. Mag. 90 (2010) 2519.

[49] K. Inukai, Y. Hotta, M. Taniguchi, S. Tomura, A. Yamagishi, J. Chem. Soc., Chem. Commun. (1994) 959.

[50] Y. Hotta, M. Taniguchi, K. Inukai, A. Yamagishi, Clay Miner. 32 (1997) 79.

[51] Y. Suzuki, Y. Tenma, Y. Nishioka, J. Kawamata, Chem.–Asian J. 7 (2012) 1170.

[52] E. R. Kleinfeld, G. S. Ferguson, Science 265 (1994) 370.

[53] Y. Lvov, K. Ariga, I. Ichinose, T. Kunitake, Langmuir 12 (1996) 3038.

[54] B. V. Lotsch, G. A. Ozin, Adv. Mater. 20 (2008) 4079.

[55] J. Hickey, N. A. D. Burke, H. D. H. Stöver, J. Membr. Sci. 369 (2011) 68.

[56] T. Okada, S. Yoshido, H. Miura, T. Yamakami, T. Sakai, S. Mishima, J. Phys. Chem. C 116 (2012) 21864.

[57] K. Ariga, Q. Li, M. J. McShane, Y. Lvov, A. Vinu, J. P. Hill, Chem. Mater. 24 (2012) 728.

[58] G. A. Ozin, K. Hou, B. V. Lotsch, L. Cademartiri, D. P. Puzzo, F. Scotognella, A. Ghadimi, J. Thomson, Mat. Today 12 (2009) 12.

[59] G. Kahr, F. T. Madsen, Appl. Clay Sci. 9 (1995) 327.

[60] S. Nir, G. Rytwo, U. Yermiyahu, L. A. Margulies, Colloid Polym. Sci. 272 (1994) 619.

[61] R. A. Schoonheydt, L. Heughebaert, Clay Miner. 27 (1992) 91.

[62] C. H. Giles, D. Smith, A. Huitson, J. Chem. Soc. 111 (1960) 3973.

[63] I. Langmuir, J. Am. Chem. Soc. 40 (1918) 1361.

[64] S. Brunauer, P. H. Emmett, E. Teller J. Am. Chem. Soc. 60 (1938) 309.

[65] G. Lagaly, Solid State Ionics 22 (1986) 43.

[66] G. Lagaly, K. Beneke, Colloid Polym. Sci. 269 (1991) 1198.

[67] G. Lagaly, Clay Miner. 16 (1981) 1.

[68] R. A. Vaia, R. K. Teukolsky, E. P. Giannelis, Chem. Mater. 6 (1994) 1017.

[69] Y. Nabetani, H. Takamura, Y. Hayasaka, T. Shimada, S. Takagi, H. Tachibana, D. Masui, Z. Tong, H. Inoue, J. Am. Chem. Soc. 133 (2011) 17130.

[70] Y. Nabetani, H. Takamura, Y. Hayasaka, S. Sasamoto, Y. Tanamura, T. Shimada, D. Masui, S. Takagi, H. Tachibana, Z. Tong, H. Inoue, Nanoscale 5 (2013) 3182.

[71] M. Ogawa, M. Hiramine, Cryst. Growth Des. 14 (2014) 1516.

Table 1. Sample list in the present study.

molar ratio of the starting mixture LiF:$MgCl_2$:SiO_2:urea	sample name
0.21:0.80:8.0:8.0	Silica1.0@Hect1
0.42:0.69:8.0:8.0	Silica1.0@Hect2
0.63:0.69:8.0:8.0	Silica1.0@Hect3
0.84:0.69:8.0:8.0	Silica1.0@Hect4

Table 2. Summary of the results of the tests in which MB and $2C_{18}$ were adsorbed onto Silica1.0@HectX samples.

Sample name	Langmuir parameters of MB adsorption		TG results on $2C_{18}$-adsorbed samples	
	Q_m [mmol/g]	K_L [10^3 L/g]	Mass loss [%]	Amount adsorbed $2C_{18}$ [mmol/g]
Silica1.0@Hect1	0.12	5.7	5.8	0.11
Silica1.0@Hect2	0.17	4.3	8.1	0.16
Silica1.0@Hect3	0.19	4.7	9.3	0.19
Silica1.0@Hect4	0.23	2.0	10.2	0.21

Figure captions

Fig. 1. SEM (left) and cross-sectional TEM (right) images of the silica and Silica1.0@HectX (X = 1, 2, 3 and 4) samples. The grain size distributions are shown in the middle of the figure.

Fig. 2. XRD patterns for the Silica1.0@HectX (X = 1, 2, 3 and 4) samples.

Fig. 3. Nitrogen adsorption-desorption isotherms (77 K) of the Silica1.0@HectX samples (X = (a) 1, (b) 2, (c) 3 and (d) 4). The circles and crosses are the adsorption and desorption data, respectively.

Fig. 4. Isotherms for the adsorption of MB onto Silica1.0@HectX (X = 1, 2, 3 and 4) samples from aqueous solutions (298 K).

Fig. 5. TG curves of the Silica1.0@HectX (X = 1, 2, 3 and 4) samples with adsorbed $2C_{18}$.

Fig. 6. Schematic of the alkylammonium ion arrangements in the interlayer space.

Fig. 7. Changes in the XRD patterns that occurred when Silica1.0@HectX (X = 1, 2, 3 and 4) samples underwent cation exchange with $2C_{18}$ bromide. The green lines are for before and the blue lines for after the cation exchange reaction.

Fig. 8. (left) Grain size distributions and (right) SEM images of Silica1.0@Hect1 (a) before and (b) after $2C_{18}$ was intercalated.

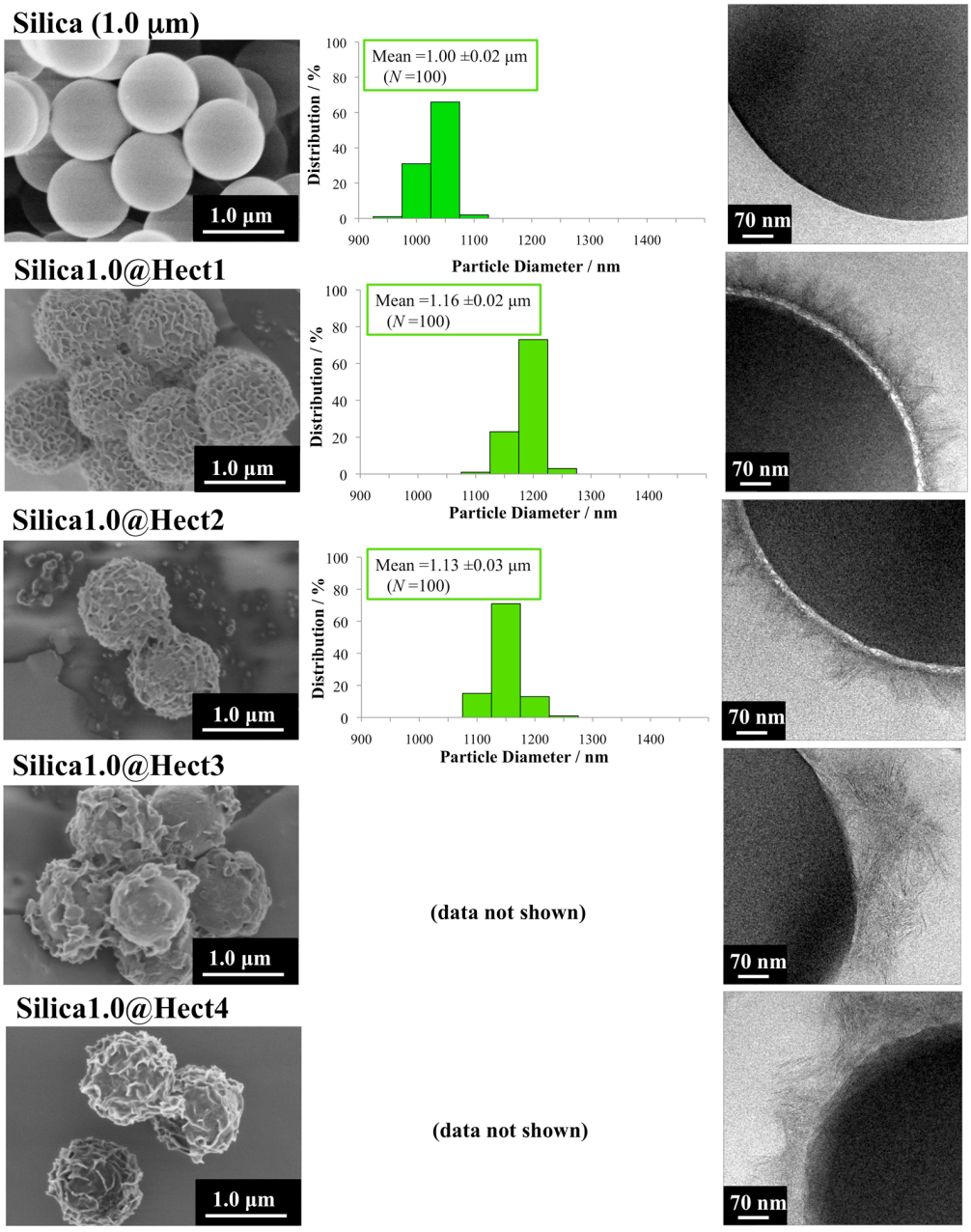

Fig. 1. SEM (left) and cross-sectional TEM (right) images of the silica and Silica1.0@HectX (X = 1, 2, 3 and 4) samples. The grain size distributions are shown in the middle of the figure.

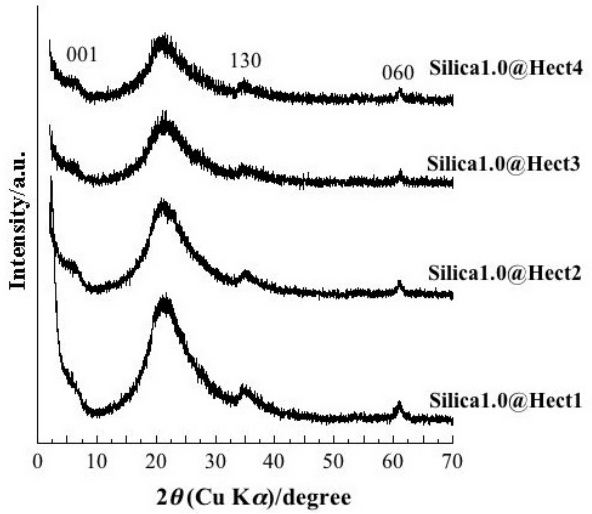

Fig. 2. XRD patterns for the Silica1.0@HectX (X = 1, 2, 3 and 4) samples.

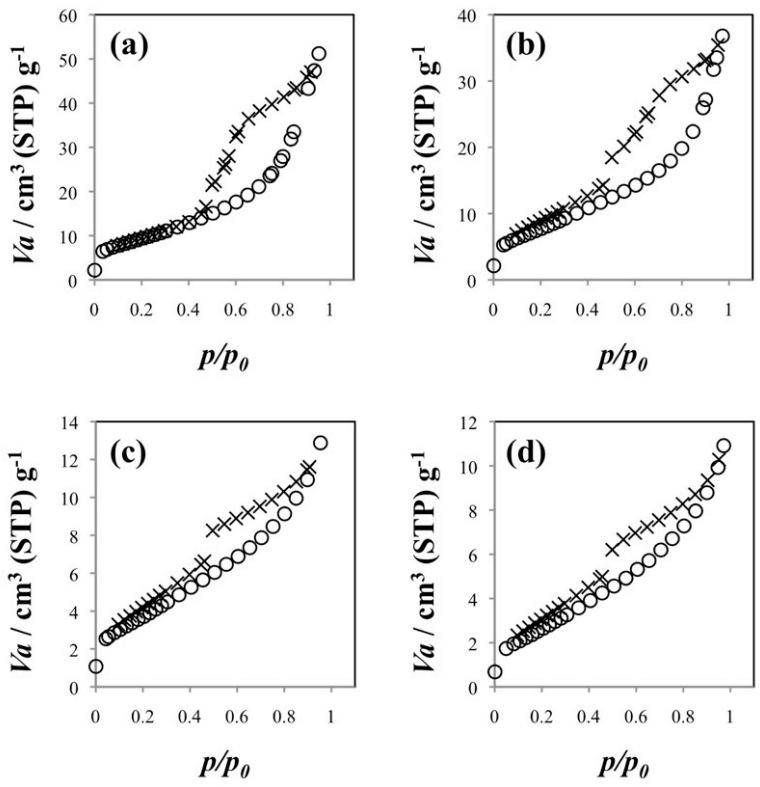

Fig. 3. Nitrogen adsorption-desorption isotherms (77 K) of the Silica1.0@HectX samples (X = (a) 1, (b) 2, (c) 3 and (d) 4). The circles and crosses are the adsorption and desorption data, respectively.

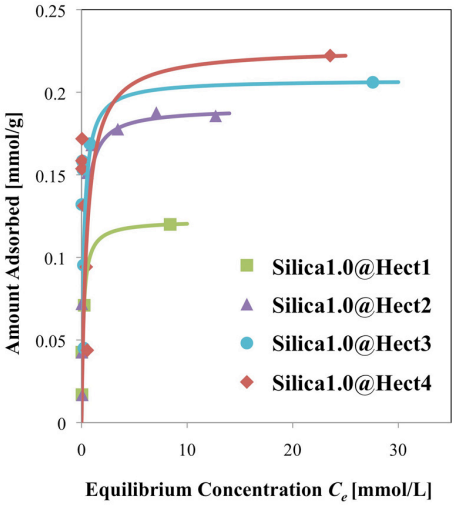

Fig. 4. Isotherms for the adsorption of MB onto Silica1.0@HectX (X = 1, 2, 3 and 4) samples from aqueous solutions (298 K).

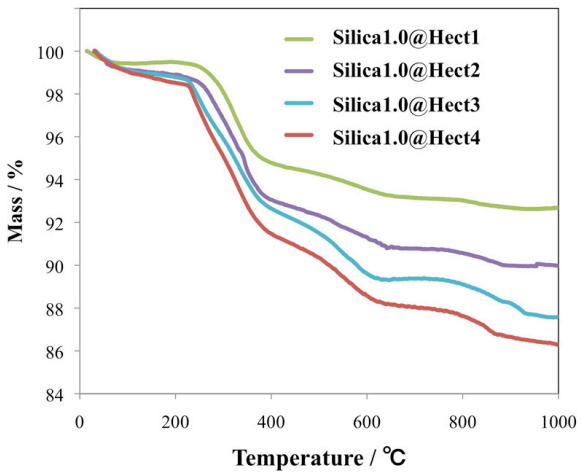

Fig. 5. TG curves of the Silica1.0@HectX (X = 1, 2, 3 and 4) samples with adsorbed $2C_{18}$.

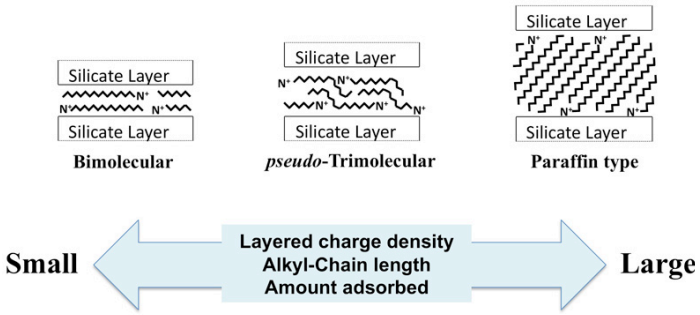

Fig. 6. Schematic of the alkylammonium ion arrangements in the interlayer space.

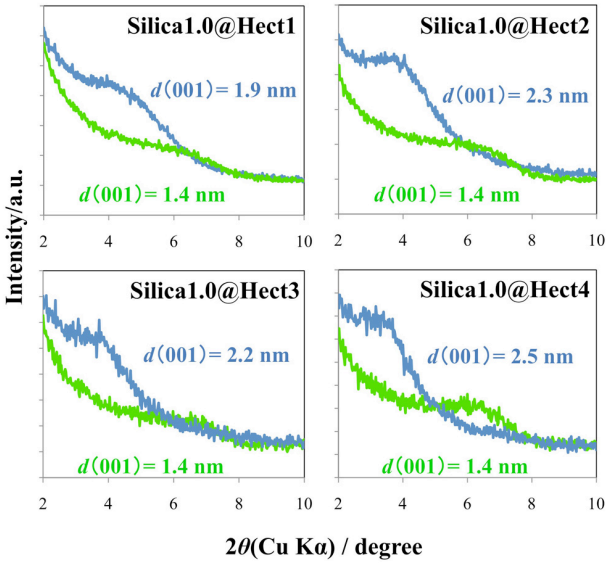

Fig. 7. Changes in the XRD patterns that occurred when Silica1.0@HectX (X = 1, 2, 3 and 4) samples underwent cation exchange with $2C_{18}$ bromide. The green lines are for before and the blue lines for after the cation exchange reaction.

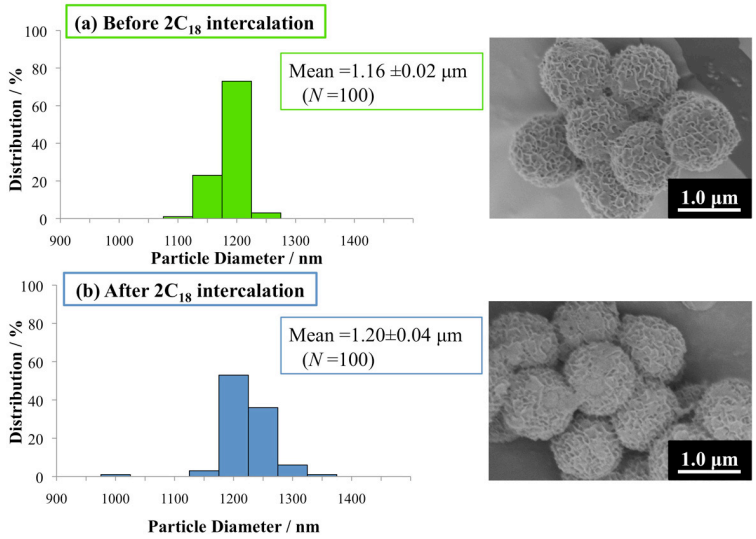

Fig. 8. (left) Grain size distributions and (right) SEM images of Silica1.0@Hect1 (a) before and (b) after $2C_{18}$ was intercalated.